Analyst

PAPER

View Article Online
View Journal

Cite this: DOI: 10.1039/d0an02126a

Self-powered liquid chemical sensors based on solid–liquid contact electrification†

Zhihua Ying, *[a,b] Yin Long,[a] Fan Yang,[a] Yutao Dong, [a] Jun Li, [a] Ziyi Zhang[a] and Xudong Wang*[a]

Received 27th October 2020,
Accepted 17th January 2021

DOI: 10.1039/d0an02126a

rsc.li/analyst

Triboelectric nanogenerators (TENGs) have attracted many research endeavors as self-powered sensors for force, velocity, and gas detection based on solid–solid or solid–air interactions. Recently, triboelectrification at liquid–solid interfaces also showed intriguing capability in converting physical contacts into electricity. Here, we report a self-powered triboelectric sensor for liquid chemical sensing based on liquid–solid electrification. As a liquid droplet passed across the tribo-negative sensor surface, the induced surface charge balanced with the electrical double layer charge in the liquid droplet. The competition between the double layer charge and surface charge generated characteristic positive and negative voltage spikes, which may serve as a "binary feature" to identify the chemical compound. The sensor showed distinct sensitivity to three amino acids including glycine, lysine and phenylalanine as a function of their concentration. The versatile sensing ability was further demonstrated on several other inorganic and organic chemical compounds dissolved in DI water. This work demonstrated a promising sensing application based on the triboelectrification principle for biofluid sensor development.

Introduction

Liquid sensing is broadly utilized in many areas including the chemical industry,[1–3] medical diagnosis,[4–6] food manufacturing,[7–9] and environmental protection.[10–13] Currently, the most commonly used methods for detecting biochemical concentrations in liquids are based on electrochemical sensors,[14–17] fluorescent probes[18–20] and optical fiber sensors.[21,22] These devices are typically bulky and complex, run on an external power source, and require a relatively long time to obtain the required information. It is generally desired for a liquid sensor to provide rapid, continuous and reliable detection. Recently, contact electrification between liquid and solid films has been demonstrated as a promising methodology for inducing electric charges on solid surfaces.[23–25] This phenomenon has quickly become an intriguing design principle of a triboelectric nanogenerator (TENG) for direct electricity generation from liquid movements, such as rain drops and water waves.[26–28] Same as other TENG devices, a self-powered liquid chemical sensor can generate electrical signals through the triboelectric effect without any extra energy supply. This signal information could be directly sent to other electronics in real applications.[29–31] Thus, this immediate electricity-generation capability from liquid motion allows the implementation of this principle as a power-free sensor device that would be simple, portable or wearable, and cost effective.[32–34]

A two-step formation process of the electric double layer (EDL) at the liquid–solid interface has been proposed by Wang,[35,36] and electron transfer dominates on some materials. Based on the electrification principle, the amount of electricity generated is dependent on the dielectric property and the electronegativity of both the liquid and contacting material as well as the area of the contacting surface and the moving speed. Thus far, studies have been primarily focused on how to optimize the solid materials in order to improve the electricity generation from water droplets.[23,37–41] However, with given physical conditions of a liquid–solid interactive TENG, it is reasonable to envision that the change of the liquid composition would also induce electric output variations.[42,43] This type of change, if quantified, can provide an ideal sensing capability for liquid samples, which may offer profound application potential in liquid chemical sensing, biofluid sensing, and environmental sensing. In this article, we report a simple self-powered liquid sensor for chemical sensing based on the principle of liquid–solid contact electrification. The triboelectrification (TE)-based sensor device showed fast sensitivity to various biochemicals including glycine, lysine, phenylalanine, and interference chemicals dissolved in water. This study successfully validated the hypothesis that liquid contact electrifi-

[a]Department of Materials Science and Engineering, University of Wisconsin-Madison, Madison, WI 53706, USA. E-mail: xudong.wang@wisc.edu
[b]College of Electronics and Information, Hangzhou Dianzi University, Hangzhou, 310018, People's Republic of China. E-mail: yingzh@hdu.edu.cn

†Electronic supplementary information (ESI) available. See DOI: 10.1039/d0an02126a

cation may lead to a new liquid sensing strategy for portable, wearable and self-powered biofluid sensor development.

Results and discussion

The working principle of the self-powered biofluid sensor is based on the contact electrification principle between the testing liquid droplets and the PTFE surface. As shown in Fig. 1A, the sensor surface was a PTFE thin film for liquid reception. Two copper electrodes on the back side were set for outputting the triboelectric voltage signal. The electrode at the lower position was the sensing electrode to collect electrification-induced charges, while the top electrode was used as the reference electrode. Water charge is always positive but its magnitude is related to the material position in most triboelectric series, in which PTFE is a highly negative material;[44,45] when a liquid droplet contacts the PTFE surface, negative charges are induced at the PTFE surface and the droplet becomes positively charged. Opposite charges could also form in the vicinity of the charged liquid surface as an electrochemical double layer. During the initial movement of the liquid droplet, local charges will establish an equilibrium distribution, in which the positive liquid surface charge is balanced by the PTFE surface charge (σ_s) and liquid internal charge (σ_l) (Fig. 1A-I). As the droplet moves over the electrode covered area, the negative charges on the PTFE surface induce a positive charge on the sensing electrode, generating a positive voltage peak over a load connected between the sensing and reference electrodes (Fig. 1A-II). Once the droplet passes the sensing electrode region, the induced charges become unbalanced, and thus a negative potential difference builds up to drive electrons back to the sensing electrode. This local electronic fluctuation may also disturb the electrochemical double layer distribution, and thus releases more positive charges to be balanced by the sensing electrode (Fig. 1A-III). Therefore, a larger amount of charges (or high local potential) could be induced in this stage compared to stage II. The electric equilibrium will eventually be re-established after the droplet moves away from the sensing area (Fig. 1A-IV). The corresponding voltage output profile of one cycle is shown in Fig. 1B, illustrating a biphasic waveform with a significantly higher negative voltage peak value compared to the positive peak. Integrating the peak area represents the amount of charge flowing through the load, which also revealed that the charge flow in stage III was about twice as much as that in stage II. Besides, the time (Δt) from 0 V to the maximal value was only 0.02 s, demonstrating a fast sensing response.

Based on the mechanism, the voltage peak intensity would be related to the time taken for the liquid droplet to pass through the electrode area, or how fast the charges may be balanced. To reveal this relationship, the moving speed was controlled by tilting the sensor plate at different angles. First, it was found that both positive and negative voltage peaks were rather stable as the tilting angle was fixed. At a tilting angle of 30°, the average negative voltage peak was −0.020 ± 0.001 V. The small voltage amplitude was likely due to the slow motion of the droplet, which induced a slow charge accumulation. As the tilting angle increased to 45°, the average negative voltage peaked at −0.116 ± 0.008 V, which only slightly decreased to −0.096 ± 0.010 V as the tilting angle increased to 60° and then rapidly dropped to −0.014 ± 0.002 V at a tilting angle of 75°. However, the positive voltage peaks remained at a fairly stable value of ~0.02 V at all these tilting angles (Fig. 2A). The nearly constant positive peaks evidenced the reaching of the equilibrium state before the droplet arriving at the sensing electrode, and thus a small amount of charge would be induced in stage II. The significantly enhanced negative peak

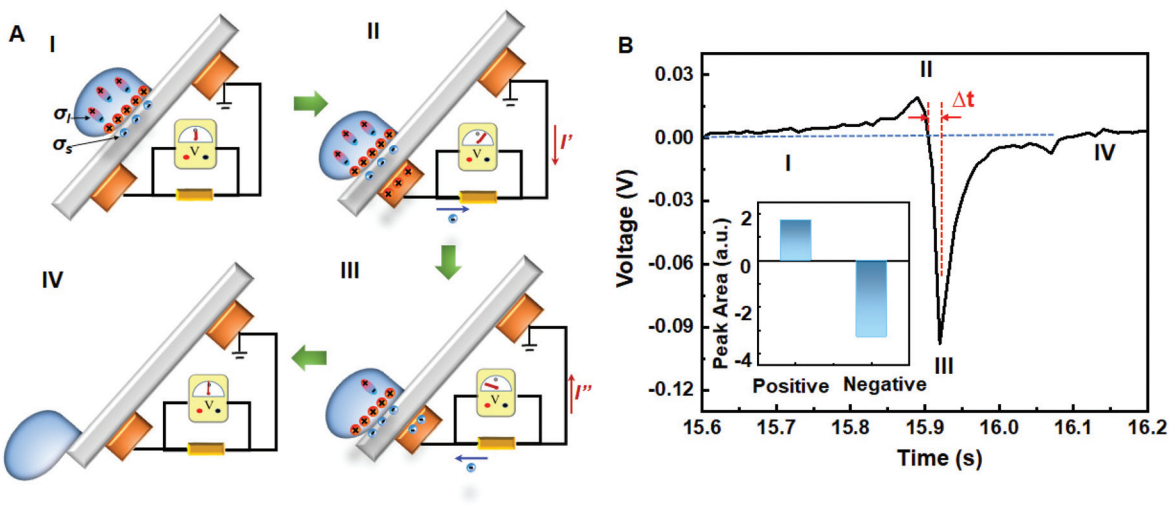

Fig. 1 Mechanism of the TE-based liquid sensor. (A) Schematic illustration of the working principle of the TE-based sensor as a liquid droplet flowing across the sensor surface. (B) A typical voltage output profile of the TE-based sensor under the flow of one single water droplet. The inset shows the integrated peak area under positive and negative voltage peaks.

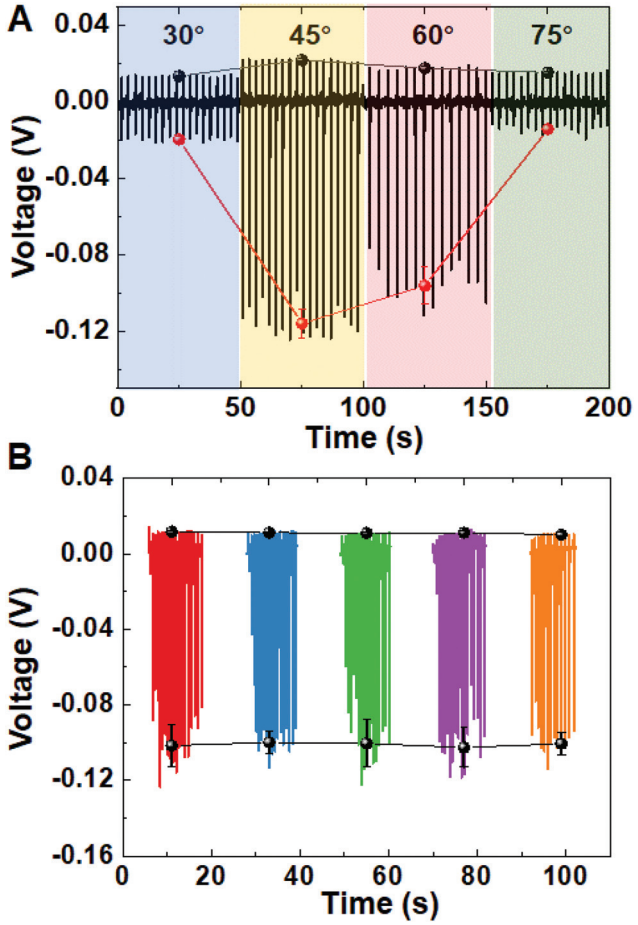

Fig. 2 Voltage signals of the TE-based liquid sensor. (A) Voltage signals of a TE-based liquid sensor at different tilting angles. (B) Repeated voltage output signals recorded from the TE-based sensor at 45° tilting angle over five different times.

intensity at 45° suggested that an appropriate time of interaction between the droplet and sensing electrode was needed to maximize the charge to be released from the double layer trapping. The rapid drop of the negative voltage at a higher tilting angle could be attributed to the insufficient interaction for releasing the trapped charge. This result proved that the droplet travel speed was an important factor that controlled the voltage output. Therefore, in order to obtain the maximum output signal of sensing response, all the sensing experiments were conducted at 45° tilting angle (the velocity was quantified by an alternative design, ESI S2†), and a 1.25 ± 0.23 nA tribocurrent was obtained as shown in Fig. S3.† By applying droplets repeatedly from the same position, consistent voltage outputs of −0.1 ± 0.01 V were obtained. This process was repeated over five different times, and the voltage output exhibited a nearly constant value from each group of measurements with a variation within 3% of the signal value (Fig. 2B), confirming the good repeatability of the sensing responses. It should be noted that although the contact area of a droplet and PTFE may also be affected by the tilting angle,[46] it had negligible impact on moving speed quantification. This is because the speed was only determined by the time difference between the two voltage peaks when the liquid droplet passed the two electrodes and the distance between the two electrodes, which were not affected by the contact area.

The voltage generation mechanism suggests that the amount of induced charge was also related to the relevant electronegativity of the liquid droplet compared to PTFE. Many other physical conditions, such as the tilting angle, flowing distance, and droplet volume, would change the voltage amplitude. When all these conditions were fixed, the results would be able to reflect the (di)electric property of the droplet, thereby providing a selective sensing capability. Here, we select amino acids, a group of very important biological substances,[47–49] as an example to show the self-powered selective sensing capability of the TE-based liquid sensors. Three essential amino acids (Table S2†) were selected for two reasons: structure and biomedical applications, and significance of disease diagnosis. Glycine, the one with the simplest chemical structure in amino acids, has anti-inflammatory and immunomodulatory functions, and is also an insulin secretagogue.[50] Lysine, the one with an aliphatic side chain, is considered as a potential biomarker for renal cell carcinoma, and plays a key role in the neurotoxicity of amyloid b-protein in Alzheimer's disease (AD).[51] Phenylalanine, the one with an aromatic side chain, is related to immune activation in the pathogenesis of AD.[52,53] Therefore, these three types of amino acids are representative and adequate to support the hypothesized sensing capability.

In order to quantitatively evaluate the performance of the TE-based sensor for the selected amino acids, the voltage outputs were recorded from amino acid droplets with different concentrations. The highest concentration was chosen according to the solubility of the specific amino acids. Each measurement on each concentration value was conducted for at least 15 seconds (*i.e.*, 20 droplets). For comparison, DI water droplets were also tested with each group of amino acid samples. As shown in Fig. 3, the DI water droplets yielded the highest negative voltage peak at ~−0.1 V compared to all three amino acid samples. Significant changes in the negative voltage peaks were observed as the concentration changed, while the positive peaks remained in a fairly small range of variation. In general, both positive and negative voltage peaks decreased as the concentration increased for all amino acids (Fig. 3A–C). The negative voltage peaks exhibited a significantly larger change compared to the positive voltage peaks. As shown in Fig. 3D–F, the average negative voltage peak values at each concentration point were plotted for each amino acid and were good fits to a logarithm curve (Table S3†). As the positive peak intensity was directly related to σ_s, the increase of the amino acid concentration had little impact on the balanced σ_l and σ_s values. Therefore, the positive peak intensity showed a very small variation (decreasing) as the amino acid concentration increased across the entire testing range. The large decrease of the negative voltage peak intensity could be attributed to the stabilization of the electrochemical double layer in the liquid

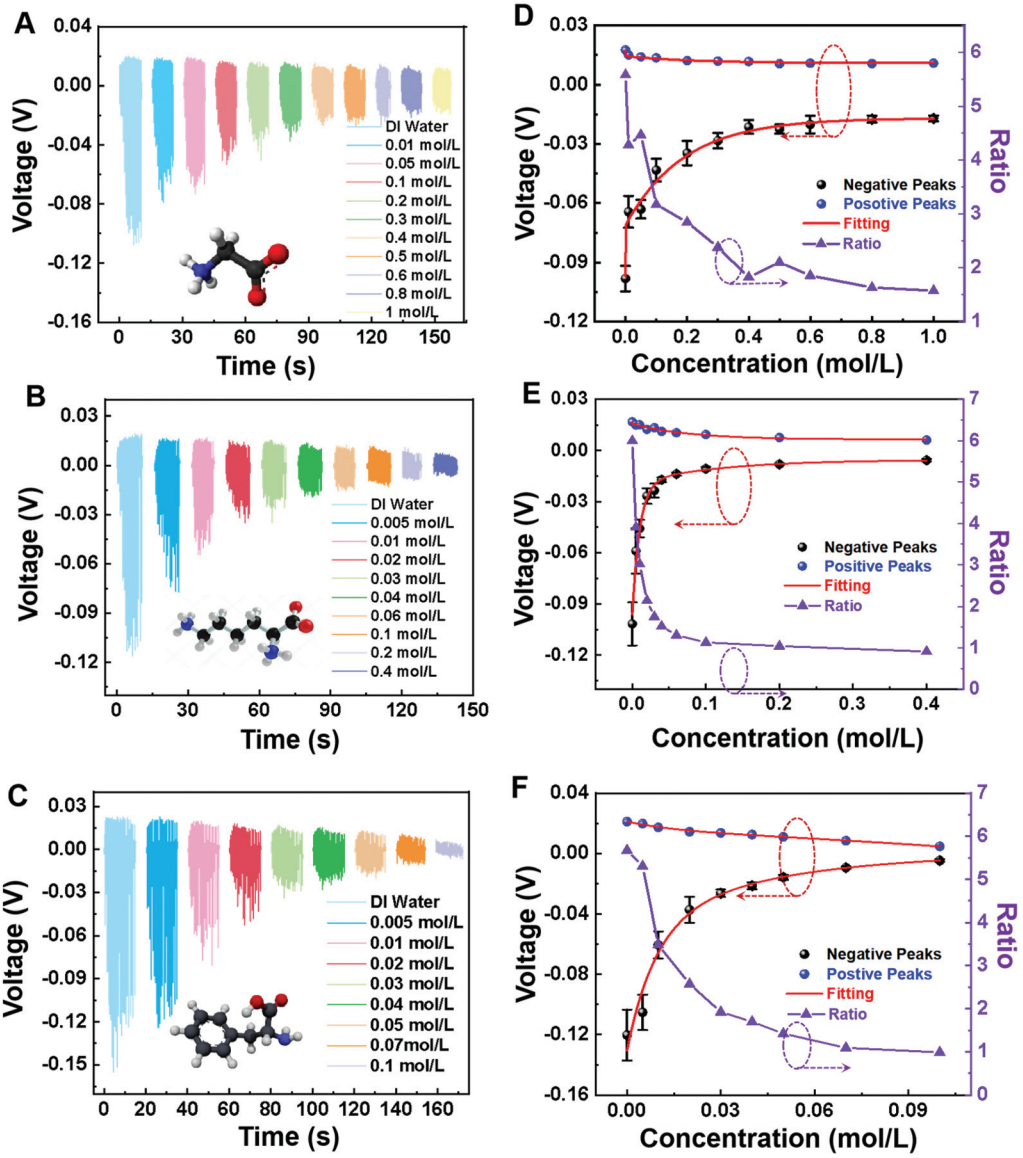

Fig. 3 Voltage responses of the TE-based liquid sensor to three amino acids. The voltage output signals of the TE-based sensor to glycine (A), lysine (B) and phenylalanine (C) aqueous solutions measured at a series of concentrations, respectively. (D–F) The corresponding plots of the voltage peak values as a function of the concentration of glycine, lysine, and phenylalanine, respectively.

droplet when an additional amount of amino acid was added. The ratios of the positive to negative peak intensity were all eventually reaching a unit, suggesting that an equal amount of charge flow was established at high concentrations. This phenomenon revealed that as the double layer was eventually stabilized, both back and forth charge flows were only contributed to σ_s.

One should notice that although the general principle was the same and so as similar trends were obtained, the three amino acids demonstrated distinguishing voltage change patterns. The changing rate and the ratio between the positive and negative peak values would reflect the molecules' chemical and dielectric nature. Therefore, these two patterns together may be considered as a "binary feature" to identify the molecules. Compared to lysine and phenylalanine, glycine has a relatively simple chemical structure and does not have any large side chains (Table S2†). Since the $-NH_2$ group is always positively charged in a solution, more $-NH_2$ groups in the molecule would yield more or stronger electric dipoles in the solution when triboelectric charges were induced. Therefore, as the droplet moved away from the sensing electrode, more/stronger in-solution dipoles would lead to a stronger interaction at the droplet surface and stabilize the induced surface charge (σ_l); the obtained highest sensitivity is shown in Fig. S5.† As less σ_l is being released, the negative peak would be more relative to σ_s and thus closer to the value of the positive peak, moving their ratio closer to unity. The presence of a nonpolar and large aromatic side chain in phenylalanine

could be the reason for the most significant decrease of the positive peak as its concentration increases.

The above results revealed that an increase in the ion concentration leads to the suppression of the transferred charge amount. To further demonstrate the strong and versatile sensing ability of our TE-based liquid sensor, we tested the voltage responses from a broader range of chemicals, including ethanol, NaCl, acetic acid, PBS and Na_2CO_3. Urea, a breakdown product of amino acids, was not selected because it is neither acidic nor alkaline when it dissolves in water. All of these solutions were prepared with a concentration of 0.1 mol L^{-1} in DI water. DI water and tap water (which contains several types of ions) were also detected for comparison. The corresponding voltage output profiles are shown in Fig. 4A. It can be seen that DI water still had the maximum voltage output due to the minimal free ions in the solution, as expected. A similar voltage profile (with a slight decrease in the negative voltage peak) was obtained from ethanol solution, possibly due to its similar protic behavior. Tap water, as it contained a lot more free ions, generated a much lower negative voltage peak compared to those from DI water droplets. The three ionic solutions, NaCl, acetic acid and Na_2CO_3, exhibited the lowest voltage peaks, both negative and positive, and their ratios were nearly unity, as shown in Fig. 4B. This phenomenon is consistent with our proposed mechanism that free ions stabilized the double layer in the liquid droplet (*i.e.*, σ_l), and the negative voltage was largely determined by σ_s alone.

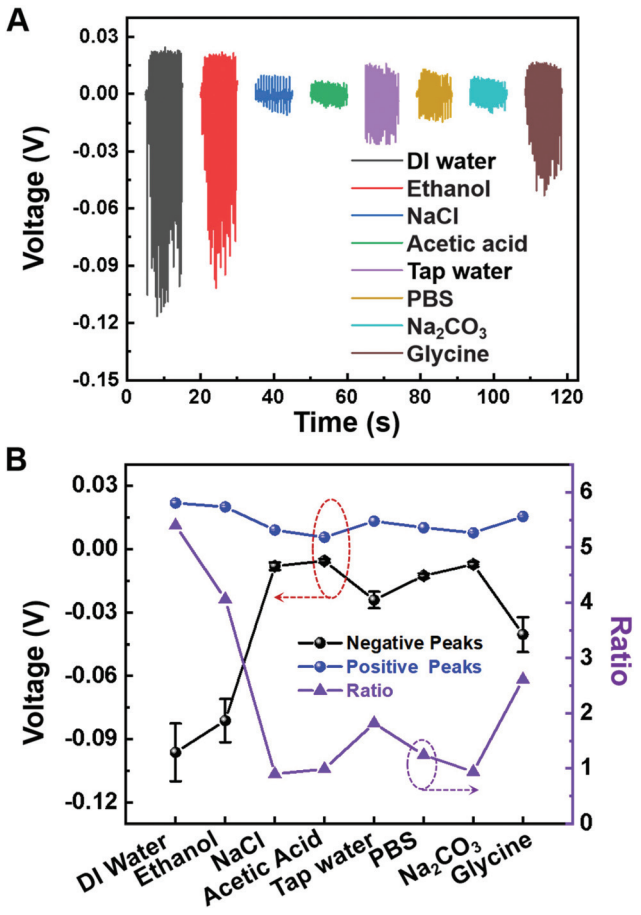

Fig. 4 Sensing capability of a TE-based liquid sensor to different analytes. (A) Voltage responses of the TE-based liquid sensor when droplets of DI water, ethanol, NaCl, acetic acid, tap water, PBS, Na_2CO_3 and glycine were added to the sensor surface. Except water, other analytes were prepared with a concentration of 0.1 mol L^{-1} in DI water. (B) Values of the positive and negative voltage peaks for different analytes and the ratio between the positive and negative peak values.

Conclusions

In summary, we developed a self-powered triboelectric sensor based on liquid–solid electrification for liquid chemical sensing. The sensor was built on a triboelectric negative surface with two back Cu electrodes for charge induction. As the liquid droplet passed over the sensor surface, positive charges were induced at the liquid surface, which were balanced by the electrical double layer charge in the liquid and the surface charge from the sensor. As the liquid droplet passed through the sensing electrode, the competing release of the double layer charge and surface charge generated characteristic positive and negative voltage spikes, which signaled the liquid chemistry. We tested the sensing responses to three different types of amino acids, including glycine, lysine and phenylalanine. The negative voltage peaks demonstrated a strong concentration relationship, which decreased logarithmically as the concentration increased. We further showed the sensor behavior to several organic and inorganic chemicals. The characteristic negative and positive voltage peaks and their amplitude ratio also confirmed the strong correlation to free ion concentrations. Therefore, we believe that in our triboelectric liquid sensor, the multiple sources of surface charge generation and balancing could provide distinct positive and negative voltage outputs directly correlating to the liquid chemistry. This phenomenon may potentially serve as a "binary feature" for chemistry identification in liquid solution with more comprehensive quantification. This liquid sensor design, together with its surface-charge-determined sensing principle, offers great promise for the development of effective and low-cost sensor technology for liquid systems.

Experimental section

Materials

Glycine (98.5+%), L-lysine (≥98%), L-phenylalanine (≥98%), acetic acid (≥98%) and sodium carbonate (Na_2CO_3, ≥99.5%) were purchased from Millipore Sigma Co. Sodium chloride (NaCl, ≥99.0%) was obtained from Alfa Aesar Co. Ethyl alcohol 200 Proof was purchased from Pharmco by Greenfield Global Inc. Phosphate buffered saline (PBS, Tissue Culture Grade) was purchased from Crystalgen Inc. The polytetrafluoroethylene (PTFE) film was obtained from CS Hyde Co.

Fabrication of the self-powered liquid sensor

The method used to fabricate the TENG-based sensor is shown in Fig. S1.† A rectangular PTFE film (90 μm in thickness, 1 cm wide and 7 cm long) was washed in acetone, ethanol and DI water for 15 min each. Two Cu electrodes 22 μm in thickness were deposited by e-beam evaporation (CHA-600) on the backside of the PTFE film. The top Cu electrode had a size of 0.2 cm × 0.5 cm and the lower Cu electrode was 1 cm × 0.5 cm in size. The two Cu electrodes were spaced by 5 cm. The top electrode was positioned in the middle of the PTEF film to avoid direct liquid droplet contact.

Sensor characterization

As shown in Fig. S3,† a separating funnel (125 mL in volume) was used to contain the liquid sample and provide continuous liquid droplets toward the PTFE film with a stable dropping frequency. The funnel outlet was positioned 0.5 cm above the PTFE film and 0.5 cm ahead of the first Cu electrode. The droplets coming out of the funnel outlet all had a consistent volume of 0.05 ml. The voltage outputs of the TE-based sensor between the two Cu electrodes were measured using a low-noise amplifier (Stanford Research Systems, Model SR560). Contact angles were measured using a Dataphysics OCA 15 Optical Contact Angle Measuring System. A Zeiss LEO 1530 Schottky-type field-emission scanning electron microscope was used to image the morphologies of the samples.

Author contributions

Zhihua Ying: conceptualization, methodology, visualization, data curation, and writing the original draft. Yin Long: conceptualization, methodology, and writing the original draft. Fan Yang: validation and software. Yutao Dong: conceptualization. Jun li: methodology. Ziyi Zhang: investigation. Xudong Wang: conceptualization, methodology, supervision, and writing – review and editing.

Conflicts of interest

There are no conflicts to declare.

Acknowledgements

This work was primarily supported by the National Science Foundation (DMR-1709025). Z. Y. is grateful for the financial support from the China Scholarship Council.

References

1 C. Bai, J. Zhang, R. Quo, Q. Zhang, M. Mei, M. Chen, B. Wei, C. Wang and C. Qu, *Ind. Eng. Chem. Res.*, 2020, **59**, 8125–8135.
2 R. Boroujerdi, A. Abdelkader and R. Paul, *Nano-Micro Lett.*, 2020, **12**, 33.
3 B. Huy, H. P. Van, D. V. Pham, T. H. C. Hoang, T. B. Pham, T. C. Do, Q. M. Ngo and T. V. Nguyen, *Environ. Technol. Lett.*, 2019, **40**, 3403–3411.
4 S. Rassel, C. Xu, S. Zhang and D. Y. Ban, *Analyst*, 2020, **145**, 2441–2456.
5 Q. Fan, L. Wang, D. Xu, Y. Duo, J. Gao, L. Zhang, X. Wang, X. Chen, J. Li and H. Zhang, *Nanoscale*, 2020, **12**, 11364–11394.
6 Y. M. Park, Y. S. Choi, H. R. Lee, Y. S. Heo, N. H. Bae, T. J. Lee and S. J. Lee, *Biosens. Bioelectron.*, 2020, **161**, 112252.
7 F. Laghrib, M. Bakasse, S. Lahrich and M. A. El Mhammedi, *Mater. Sci. Eng., C*, 2020, **107**, 110349.
8 O. Cakir, M. Bakhshpour, F. Yilmaz and Z. Baysal, *Mater. Sci. Eng., C*, 2019, **102**, 483–491.
9 H. Mahmoudi-Moghaddam, S. Tajik and H. Beitollahi, *Food Chem.*, 2019, **286**, 191–196.
10 L. Yang, Y. L. Liu, C. G. Liu, F. Ye and Y. Fu, *J. Hazard. Mater.*, 2020, **381**, 120966.
11 E. Shojaei, M. Masrournia, A. Beyramabadi and H. Behmadi, *Int. J. Environ. Anal. Chem.*, 2020, **3**, 1–16.
12 X. Fang, B. Zong and S. Mao, *Nano-Micro Lett.*, 2018, **10**, 64.
13 G. Chakraborty, P. Das and S. K. Mandal, *ACS Appl. Mater. Interfaces*, 2018, **10**(49), 42406–42416.
14 Y. Yao, X. X. Liu, Y. Z. Shao, Y. B. Ying and J. F. Ping, *Biosens. Bioelectron.*, 2020, **66**, 112463.
15 P. Singh, S. K. Pandey, J. Singh, S. Srivastava, S. Sachan and S. K. Singh, *Nano-Micro Lett.*, 2016, **8**, 193–203.
16 F. Li, Z. Yu, X. Han and R. Lai, *Anal. Chim. Acta*, 2019, **1051**, 1–23.
17 Y. Zhang and X. Chen, *Nanoscale*, 2019, **11**, 19105–19118.
18 H. Qi, M. Teng, M. Liu, S. Liu, J. Li, H. Yu, C. Teng, Z. Huang, H. Liu, Q. Shao, A. Umar, T. Ding, Q. Gao and Z. Guo, *J. Colloid Interface Sci.*, 2019, **539**, 332–341.
19 Y. Wang, S. Lao, W. Ding, Z. Zhang and S. Liu, *Sens. Actuators, B*, 2019, **284**, 186–192.
20 X. Wu, H. Wang, S. Yang, H. Tian, Y. Liu and B. Sun, *Food Chem.*, 2019, **284**, 23–27.
21 Y. Zhang, Y. Sun, L. Cai, Y. Gao and Y. Cai, *Measurement*, 2020, **158**, 107742.
22 Y. Zhang, T. Zhou, B. Han, A. Zhang and Y. Zhao, *Nanoscale*, 2018, **10**, 13832–13856.
23 D. Choi, D. W. Kim, D. Yoo, K. J. Cha, M. La and D. S. Kim, *Nano Energy*, 2017, **36**, 250–259.
24 W. Tang, B. D. Chen and Z. L. Wang, *Adv. Funct. Mater.*, 2019, 1901069.
25 S. Chatterjee, S. R. Burman, I. Khan, S. Saha, D. Choi, S. Lee and Z.-H. Lin, *Nanoscale*, 2020, **12**, 17663–17697.
26 W. Xu, H. Zheng, Y. Liu, X. Zhou, C. Zhang, Y. Song, X. Deng, M. Leung, Z. Yang, R. X. Xu, Z. L. Wang, X. C. Zeng and Z. Wang, *Nature*, 2020, **578**, 392–396.
27 Y. Long, Y. Yu, X. Yin, J. Li, C. Carlos, X. Du, Y. Jiang and X. Wang, *Nano Energy*, 2019, **57**, 558–565.
28 G. Zhu, Y. Su, P. Bai, J. Chen, Q. Jing, W. Yang and Z. L. Wang, *ACS Nano*, 2014, **8**(6), 6031–6037.

29 X. Li, M. H. Yeh, Z. H. Lin, H. Guo, P. K. Yang, J. Wang, S. Wang, R. Yu, T. Zhang and Z. L. Wang, *ACS Nano*, 2015, **9**(11), 11056–11063.
30 L. Zheng, Y. Wu, X. Chen, A. Yu, L. Xu, Y. Liu, H. Li and Z. L. Wang, *Adv. Funct. Mater.*, 2017, **27**, 1606408.
31 H. Wang, Z. Xiang, P. Giorgia, X. Mu, Y. Yang, Z. L. Wang and C. Lee, *Nano Energy*, 2016, **23**, 80–88.
32 S. Jang, M. La, S. Cho, Y. Yun, J. H. Choi, Y. Ra, S. J. Park and D. Choi, *Nano Energy*, 2020, **70**, 104541.
33 Z. Yuan, X. Du, H. Niu, N. Li, G. Shen, C. Li and Z. L. Wang, *Nanoscale*, 2019, **11**, 495–503.
34 W. Tang, T. Jiang, F. Fan, A. Yu, C. Zhang, X. Cao and Z. L. Wang, *Adv. Funct. Mater.*, 2015, **25**, 3718–3725.
35 Z. L. Wang and A. C. Wang, *Mater. Today*, 2019, **30**, 34–51.
36 S. Lin, X. Chen and Z. L. Wang, *Nano Energy*, 2020, **76**, 105070.
37 Y. Wang and Y. Yang, *Nano Energy*, 2019, **56**, 547–554.
38 X. Chen, Q. Xu, S. Bai and Y. Qin, *Nano Energy*, 2017, **33**, 288–292.
39 L. Zhang, N. Zhang, Y. Yang, S. Xiang, C. Tao, S. Yang and X. Fan, *ACS Appl. Mater. Interfaces*, 2018, **10**(36), 30819–30826.
40 X. Cui, H. Zhang, S. Cao, Z. Yuan, J. Ding and S. Sang, *Nano Energy*, 2018, **52**, 71–77.
41 Z. H. Lin, G. Cheng, S. Lee, K. C. Pradel and Z. L. Wang, *Adv. Mater.*, 2014, **26**, 4690–4696.
42 S. Lin, L. Xu, A. C. Wang and Z. L. Wang, *Nat. Commun.*, 2020, **11**, 399.
43 J. Nie, Z. Ren, L. Xu, S. Lin, F. Zhan, X. Chen and Z. L. Wang, *Adv. Mater.*, 2019, 1905696.
44 T. A. L. Burgo, F. Galembeck and G. H. Pollack, *J. Electrost.*, 2016, **80**, 30–33.
45 P. Jiang, L. Zhang, H. Guo, C. Chen, C. Wu, S. Zhang and Z. L. Wang, *Adv. Mater.*, 2019, 1902793.
46 I. Ríos-Lópeza, S. Evgenidisa, M. Kostogloua, X. Zabulisb and T. D. Karapantsios, *Colloids Surf., A*, 2018, **549**, 164–173.
47 F. S. Mjalli, *J. Taiwan Inst. Chem. Eng.*, 2016, **61**, 64–74.
48 H. Uneyama, H. Kobayashi and N. Tonouchi, *Adv. Biochem. Eng. Biotechnol.*, 2017, **159**, 273–287.
49 S. Dato, E. Hoxha, P. Crocco, F. Iannone, G. Passarino and G. Rose, *Biogerontology*, 2019, **20**, 17–31.
50 M. Zenil-Vega, E. Ceron, G. Lopez-Bello, J. Moreno, E. Juarez-Cruz, M. Castillejos-Lopez, D. Bernal-Alcantara, B. Sommer and N. Alvarado-Vasquez, *Clin. Nutr.*, 2020, **39**(10), 3019–3023.
51 A. Arendowski and T. Ruman, *Anal. Methods*, 2018, **10**, 5398–5405.
52 P. Wissmann, S. Geisler, F. Leblhuber and D. Fuchs, *J. Neurol. Sci.*, 2013, **329**, 29–33.
53 N. Ermiş, L. Uzun and A. Denizli, *J. Electroanal. Chem.*, 2017, **807**, 244–252.